Comparative study of SiPM arrays performances for neutron detectors

Jessica Delgado, Felix Pino, Sandra Moretto, Daniele Corti, Alessandro Griggio, Matteo Polo, Lucio Panchieri and Daniela Fabris

***Abstract*—The SiPM market has significant growth due to its expanding applications in fields like medical imaging and nuclear physics. With various manufacturers offering SiPMs, each with unique features, there is a need for evaluating their performances. This work conducts a performance study of two medium-sized organic scintillators (EJ-309 and EJ-276G) coupled to SiPM arrays from three different brands (AdvanSiD-NUV hybrid, MPPC Hamamatsu S14161-6050HS-0, and Ketek PA3325-WB-0404). Performance evaluation is focused on energy resolution, time resolution, and the ability to discriminate between γ-rays and fast neutrons. The results indicate that the Hamamatsu SiPM array outperforms the other two SiPM arrays across all studied characteristics, achieving the lowest energy and time resolutions and the highest Figure of Merit. Nevertheless, normalizing to the number of photoelectrons created in each SiPM array per pulse, the Ketek SiPM array demonstrated the best performance in terms of energy resolution and similar timing and discrimination performances with respect to the other two arrays. This analysis provides valuable insights for selecting the right SiPM array and scintillator combination for specific applications.**

***Index Terms*—neutron detection, n/γ discrimination, SiPM-arrays.**

I. Introduction

THE rapid evolution of silicon photomultiplier (SiPM) technology has opened up exciting possibilities for investigating the replacement of conventional photomultipliers (PMTs) with Silicon Photomultipliers (SiPMs) as light converters across diverse applications, including high-energy physics, particle physics, medical imaging, astronomy, hazard detection, and more [1]–[3]. One particularly promising domain is their integration into radiation detectors when coupled with scintillators [4]. SiPMs represent a class of high-sensitivity, high-efficiency light sensors with the remarkable ability to detect light spanning from near ultraviolet to near-infrared wavelengths. These devices are composed of an array of sensitive micro-cells, all interconnected in parallel. Each micro-cell functions as a Geiger-Mode avalanche photodiode, operating beyond the breakdown voltage and featuring a resistor for passive quenching [5].

In contrast to traditional PMTs, SiPMs draw attention due to their exceptional features, including high photon detection efficiency (the typical photon detection efficiencies of the AdvanSiD, Hamamatsu, Ketek SiPM arrays, and a standard PMT at 400 nm are 43%, 48%, 43%, and 26%, respectively), significant amplification at low voltage levels, compact design, and robust immunity to magnetic fields [6], [7]. Furthermore, it is noteworthy that SiPMs are becoming increasingly affordable even as their technological expertise continues to advance. However, SiPMs do present certain challenges, including longer single photon response duration and comparatively higher noise levels attributed to dark pulses and after-pulsing. Dark pulses arise from thermally generated electrons initiating avalanches in high-field regions, while after-pulsing is triggered by the release of trapped charges within the silicon crystal, leading to a secondary avalanche within the same micro-cell. The occurrence of these phenomena is influenced by pixel recovery times, as discussed in [8], [9]. Another challenge encountered in SiPMs arises when covering extensive areas, leading to high capacitance, and consequently, the need for pre-amplification stages. This can be a problem in applications requiring fast response times, fast signal decay times, and minimal cross-talk or afterpulsing. However, despite these inherent noise characteristics, SiPMs have demonstrated impressive outcomes in sensitivity, efficiency, and particle discrimination capabilities.

The market for SiPM arrays is diverse, with prominent manufacturers offering distinct SiPM array options, each characterized by unique performance parameters. Notable examples include Hamamatsu SiPM arrays, known for their high photon detection efficiency, rapid timing resolution, and low dark count rates; Onsemi, which provides SiPM arrays with high photon detection efficiency and minimal cross-talk [10]; Ketek SiPM arrays, distinguished by their low dark count rates and minimal probability of after-pulsing [11]; and AdvanSiD, offering SiPM arrays with high gain and a low probability of after-pulsing [12]. The choice of a SiPM array is contingent upon the specific application and the experimental conditions, considering the unique characteristics of each manufacturer's offerings.

To facilitate well-informed decision-making in SiPM array selection, numerous investigations have been conducted to compare their distinct attributes. For instance, M. Grodzicka-Kobylka's study [10] compared Onsemi and Hamamatsu SiPM arrays in the context of γ spectrometry, using three inorganic scintillators (LSO, BGO, and CsI:Tl). This research examined parameters such as energy resolution, linearity, and stability under varying temperatures and bias voltages. The results favored the Onsemi SiPM array, demonstrating superior performance in most aspects. Another similar study by A. Gonzalez-Montoro [13] involved a novel comparison

Jessica Delgado, Felix Pino, and Sandra Moretto are with the Department of Physics and Astronomy "Galileo Galilei", University of Padova, Via Francesco Marzolo, 8, Padova, 35121, PD, Italy, (corresponding author e-mail: jessicadelgadoalvarez@gmail.com).

Daniele Corti, Alessandro Griggio and Daniela Fabris are with the INFN-Padova Section, Via Francesco Marzolo, 8, Padova, 35131, PD, Italy

Matteo Polo and Lucio Panchieri are with the Department of Industrial Engineering, University of Trento, Via Sommarive, 9, Povo, 38123, TN, Italy

between Onsemi, Hamamatsu Photonics, and Ketek SiPM arrays. This research assessed their responses to bias voltage and temperature variations, finding similar behavior among them with slightly more pronounced effects in the Hamamatsu components. Additionally, the study explored the performance of these SiPM arrays when coupled with pixelated crystal arrays and monolithic scintillators, focusing on photon impact estimation accuracy and energy resolution. The results indicated comparable performance across all three SiPM arrays, making them suitable for molecular imaging systems.

Another critical parameter of study is the discrimination performance when a SiPM array is coupled to a scintillator with n/γ-ray discrimination capabilities. This capability holds significant relevance in various domains, including radiation monitoring applications [14] and homeland security for identifying Special Nuclear Materials (SNM) [15]. Achieving Pulse Shape Discrimination (PSD) using SiPM arrays is a challenging job, primarily because the PSD relies on reconstructing the time profile of scintillation decay. Importantly, it must be recognized that the conversion of light into charge in a SiPM does not follow the same principles as in a PMT. Several authors have demonstrated the possibility to perform neutron/gamma-ray using millimeter scale scintillators coupled to single SiPMs, obtaining good results [8], [16], [17]. However, when large area SiPMs (array of single SiPMs) are coupled to medium-sized scintillators, achieve n/γ discrimination performance comparable with the one obtained with the PMTs is still a significant challenge, as reported in [18]–[20]. Only Grodzicka et al. [21] have been able to obtain excellent results, using scintillators with excellent PSD capabilities (stilbene), with sizes up to 25 mm of diameter, and by employing analog processing of the pulses. Nevertheless, a prior study by our group demonstrated the feasibility of n/γ-ray discrimination using large-sized scintillators coupled with large-area SiPM arrays [12]. In that study, three commercial scintillators (EJ-276, EJ-309, and EJ-301) with diameters ranging from 20 to 50 mm were utilized in conjunction with two large-area SiPM arrays from AdvanSiD (NUV and RGB). Successfully, optimum n/γ-ray discrimination results were obtained for all combinations, yielding outcomes comparable to those achieved with a PMT as the read-out. Building upon these advancements, we continue our research but this time focusing on the utilization and comparison of different types of SiPM arrays.

In the present paper, we extend this comparative investigation but this time evaluating the performance of two medium-sized organic scintillators coupled to three different SiPM arrays. Each scintillator possessing n/γ-ray discrimination capabilities: a plastic, EJ-276G (25 mm diameter x 25 mm thickness), and a liquid scintillator, EJ-309 (50 mm diameter x 50 mm thickness). Both with cylindrical shapes and from Eljen Technology–Texas USA. The SiPMs arrays are: the AdvanSiD-NUV hybrid array ASD-NUV4S-P-4x4TD (17 mm x 17 mm), the MPPC Hamamatsu S14161-6050HS-04 (24 mm x 24 mm), and the Ketek PA3325-WB-0404 (13 mm x 13 mm). The assessment encompassed an analysis of energy resolution, time resolution, and n/γ discrimination performance for each configuration [18]. This work seeks to furnish comprehensive insights into the performance characteristics of these six potential configurations, offering valuable guidance to future researchers and experimenters when selecting the most suitable SiPM array for their specific applications.

II. Methods and Experimental Set-up

A. SiPM arrays

The three tested SiPM arrays include the AdvanSiD Hybrid TD Array NUV-SiPM (16 channels, 4 mm x 4 mm active area per channel), the Hamamatsu S14161-6050HS-04 (16 channels, 6 mm x 6 mm active area per channel), and the Ketek PA3325-WB-0404 (16 channels, 3 mm x 3 mm active area per channel). Refer to Fig. 1 for images of these arrays, and their key characteristics are detailed in Table I. Fig. 2 presents the Photon Detection Efficiency (PDE) of the SiPMs across different wavelengths (Overvoltage specifications are as follows: +6 V for the AdvanSiD, +2.7 V for the Hamamatsu, and +5 V for the Ketek.), along with the emission curves of the plastic and liquid scintillators. As can be seen, all three SiPM arrays encompass the wavelength emission range of the organic scintillators, with the most favorable alignment observed between the Hamamatsu SiPM and the emission peak of the liquid scintillator. To quantify the match between the sensitivity of each SiPM and the emission curves of the scintillators in Table II, a value is assigned. This value represents the convolution between the PDE of each SiPM array and the normalized emission spectrum of each scintillator. These values can be interpreted as the probability of a scintillation photon sampled from the emission spectrum to be converted into a photoelectron by the read-out device. As can be seen, the highest probability is associated with the EJ-309/Hamamatsu configuration.

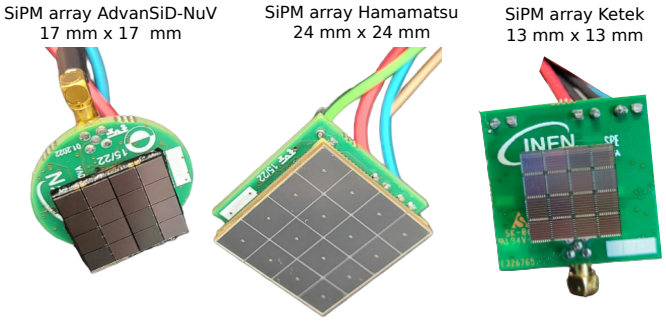

Fig. 1. Pictures of the AdvanSiD-NUV, Hamamatsu, and Ketek SiPM arrays.

B. Organic scintillators

To assess the performance of the SiPM arrays, two organic scintillators with n/γ-ray discrimination capabilities were employed: a cylindrical plastic scintillator EJ-276G (25 mm in diameter x 25 mm in thickness) and a cylindrical liquid cell scintillator EJ-309 (50 mm in diameter x 50 mm in thickness), both from Eljen Technology–Texas USA. To enhance the coupling between the detectors and the SiPM arrays (see Fig. 3), a small quantity of optical grease was applied. The EJ-309 is enclosed in a sealed, reflective container, while the EJ-276G is entirely exposed. Therefore, the plastic scintillator

TABLE I
MAIN CHARACTERISTICS OF THE SIPM ARRAYS TESTED

	AdvanSiD-NUV	Hamamatsu	Ketek
Array size	17 mm x 17 mm	24 mm x 24 mm	13 mm x 13 mm
Single SiPM size	4 mm x 4 mm	6 mm x 6 mm	3 mm x 3 mm
Channel number	16 channels	16 channels	16 channels
No. of cells/channels	9340	14331	13920
Cell size	40 μm x 40 μm	50 μm x 50 μm	25 μm x 25 μm
Recharge time	70 ns	$>$ 50 ns	80 ns
Cell capacitance	90 fF	140 fF	72 fF
Peak sensitivity wavelength	420 nm (43%)	450 nm (50%)	420 nm (45%)
Breakdown voltage, typ	26 V	38 V	24.5 V
Dark count rate	$<$ 100kHz/mm^2 @4V OV	7.5μA @4V OV	3.4μA @7V OV

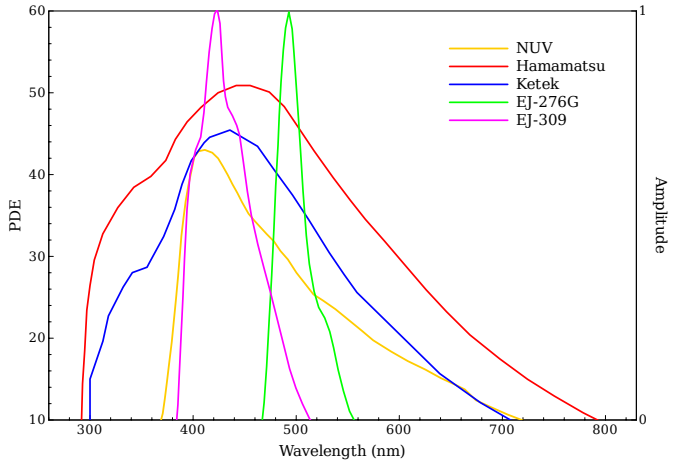

Fig. 2. Photon Detection Efficiency (PDE) corresponding to the AdvanSiD, Hamamatsu, and Ketek SiPM arrays (left axis) compared with the emission curves of the plastic and liquid scintillators (right axis). Information is taken from the manufacturers.

was carefully covered with Teflon tape, excluding the region where it is coupled to the SiPM.

Fig. 3. Picture of the EJ-276G and the EJ-309 scintillators coupled to the AdvanSiD-NUV and Hamamatsu SiPM arrays, respectively.

C. Readout board of the SiPM arrays

The SiPM array's output reading, as well as the supply of bias voltage, was executed through a specialized board designed in a sequence of four sets. Each set comprises four individual SiPMs connected in parallel. The output signals from each set undergo amplification using four trans-impedance

TABLE II
PHOTON DETECTION EFFICIENCY MULTIPLIED BY THE NORMALIZED EMISSION SPECTRUM FOR EACH SIPM ARRAY/SCINTILLATOR COMBINATION

Scintillator/SiPM array	I=$\sum_{250nm}^{900nm}$PDE(λ) $\cdot$ A(λ)$\Delta\lambda$
EJ-276G/AdvanSiD	27.3
EJ-276G/Hamamatsu	44.4
EJ-276G/Ketek	35.2
EJ-309/AdvanSiD	37.3
EJ-309/Hamamatsu	48.6
EJ-309/Ketek	42.4

preamplifiers featuring an ultra-low noise, high-speed OpAmp (LMH6629). Subsequently, these four amplified signals are combined to yield the overall output signal. To provide a clearer understanding of the circuit, a simplified diagram of the readout board is presented in Fig. 4. Each OpAmp receives voltage inputs of $\pm$2.9 V, while the applied bias voltage falls within the range of 30 to 40 V, depending on the SiPM array in use. It's important to note that the same bias voltage is applied uniformly to each SiPM.

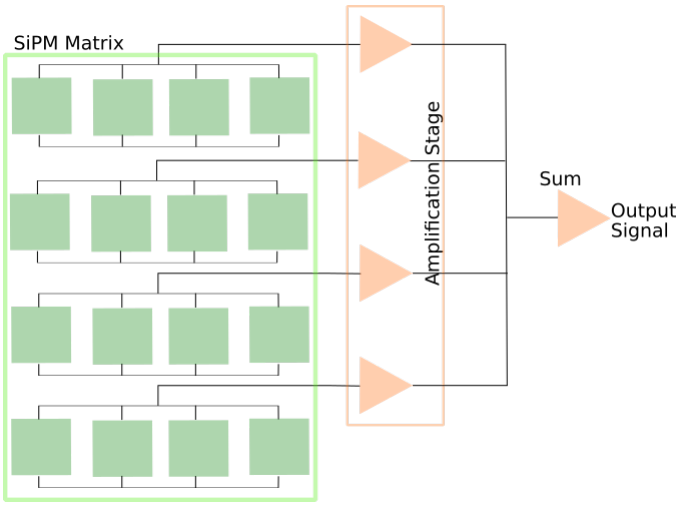

Fig. 4. Circuit diagram of the SiPM arrays' readout board.

D. Experimental details

The SiPM arrays' readout boards were powered by an Aim-TTi MX180T multi-range DC power supply. To optimize the energy resolution for each assembled detector, the overvoltage (OV) applied to each SiPM was adjusted accordingly. A bias voltage of +800 V was supplied to the PMT (R6231) of the $LaBr_3$:Ce detector used in the coincidence applications, controlled via a V6533 CAEN power supply unit connected to a USB Controller (CAEN V1718). The output signals underwent digitization using a V1730 CAEN digitizer, boasting a sampling rate of 500 MSamples/s and a 14-bit ADC resolution.

Modern digitizers are equipped with programmable FPGA (Field Programmable Gate Array) technology, allowing online pre-processing of digitized waveforms. This enables the digitizer to provide various data for each triggered event, including timestamps, total (Q_{total}), and partial (Q_{short}) waveform integrals. Additionally, digitized waveforms can be acquired and

subjected to offline data analysis. An optical fiber connection was used to control the data acquisition. The digitizer was connected to the PC using a CAEN A4818 USB 3.0 to CONET2 Adapter.

To manage electronics and data acquisition, the ABCD (Acquisition and Broadcast of Collected Data) software [22], [23], available as an open-source project, was employed. The measurements involved two γ-ray sources, ^{22}Na and ^{137}Cs (each with activities of approximately 300 kBq), as well as a n/γ-ray source ^{241}Am-^{9}Be (neutron emission rate approximately 2×10^{5} s^{-1}). Fig. 5 offers a schematic overview of the experimental setup.

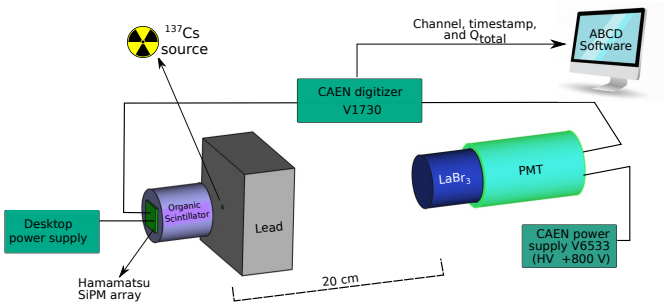

Fig. 5. Schematic view of the experimental setup, of the Hamamatsu SiPM array coupled to one of the organic scintillator, and in coincidence with $LaBr_3$:Ce detector, using the ^{137}Cs source.

E. Determination of the energy and time resolution

In this work, the energy resolution involved a Compton coincidence technique, as detailed in [24]. This method entailed setting up the neutron detector under examination in coincidence with a reference detector, specifically a $LaBr_3$:Ce detector (50 mm diameter x 50 mm thickness, from Luxium Solution), positioned face-to-face approximately 20 cm apart. Between these two detectors, a lead collimator with cuboid dimensions (10 cm x 10 cm x 5 cm) and a hole of about 1 cm in diameter was placed. The ^{137}Cs source was attached to the collimator's hole, adjacent to the organic detector.

The technique takes advantage of the fact that a 661.7 keV γ-ray emitted by the source can scatter by 180° within the active volume of the organic scintillator, depositing around 477.4 keV. Subsequently, the back-scattered γ-ray traverses the collimator's aperture reaches the reference detector and deposits its entire energy (184.3 keV). The objective is to construct the energy spectrum of events recorded by the detector under examination, in coincidence with the full-energy events corresponding to the back-scattered γ-rays detected by the $LaBr_3$:Ce detector. In this scenario, the spectrum of the assembled detector primarily comprises Compton edge events. A Gaussian fit is then applied to determine the energy resolution of the detector, calculated as $R_E = FWHM/E_0$, at E_0 equals 477.4 keV. Taking into consideration the geometry, where there is a distance of around 3 cm between the collimator and the organic scintillator, 1 keV can be attributed as the intrinsic resolution of the scattering geometry.

For the time resolution determination, a similar experimental setup was employed, but without the collimator and using a ^{22}Na source. This time, coincidences between the two 511 keV γ-rays emitted by the ^{22}Na source were recorded. An offline analysis employing a coincidence filter was conducted on digitized waveforms from each detector. The aim was to optimize the parameters (fraction and delay) of the Digital Constant Fraction Discrimination (DCFD) to attain the best time resolution. The delay parameter was varied between 10 ns and 120 ns, while for the fraction parameter three values were considered: 25%, 50%, and 75%. The final time spectrum was constructed by considering events in the full-energy peak (@511 keV) of the $LaBr_3$ detector and events with energies exceeding 200 keV in the organic scintillation detector.

F. Determination of the Pulse Shape Discrimination (PSD) capabilities

The capability of each assembled detector to discriminate between neutrons and γ-rays was assessed using an ^{241}Am-^{9}Be neutron source. Pulse shape discrimination was carried out through the double gate integration method. This approach involves the computation of the pulse shape parameter (PSP), defined as PSP = (Q_{long} - Q_{short}) / Q_{long}, where Q_{short} represents the integral over a short time window that includes the fast rise time region and part of the fastest decay component of the pulse, while Q_{long} is the integral over a long gate, encompassing the majority of the pulse, in consequence is proportional to the total light output.

Analyzing the PSP distribution enables the calculation of the Figure of Merit (FoM), defined as FoM = $\Delta/(\delta_n + \delta_\gamma)$, where Δ corresponds to the difference between the mean values of the neutron and γ-ray distributions, and (δ_n + δ_γ) represents the sum of the γ-ray and neutron Full Width at Half Maximum (FWHM). The short and long integration gates needed to be fine-tuned to maximize the FoM, indicating the best performance in terms of neutron/γ-ray discrimination. The FoM values reported in this study were determined using events falling within a light output range approximately corresponding to the Compton edge of the gamma line emitted by the ^{137}Cs source, at ∼480 keVee (electron equivalent).

III. Results and Analysis

A. Signals comparison of the SiPM arrays

As a primary step, a comparison was conducted between the output signals originating from the three SiPM arrays. To achieve this, the data acquired with the ^{137}Cs source and the EJ-276G scintillator coupled with the three different SiPM arrays under study were used. Specifically for this part the plastic scintillator measurements are reported, but for the rest of the analysis performed in this paper both plastic and liquid data are reported. In Fig. 6, it can be observed the typical waveforms for the three scenarios. These signals correspond to an event with an energy equivalent to the Compton edge of the γ-ray emitted by the ^{137}Cs source. Upon examining the waveform shapes, it becomes evident that in the three cases, the rising time is quite similar. However, there is a notable difference in the decay time, especially in the case of the Hamamatsu array, which shows a slower decay time. This discrepancy is influenced by the recharge time constant

of the SiPM microcells, which is directly related to the cell capacitance, denoted as ∼RC (refer to Table I), and the capacitance is directly proportional to the area of the microcell. This parameter characterizes how rapidly the microcells can recover after detecting a scintillation photon. It is also important to emphasize the presence of random fluctuation in the waveform generated by the Ketek configuration, characteristics that can influence the time resolution.

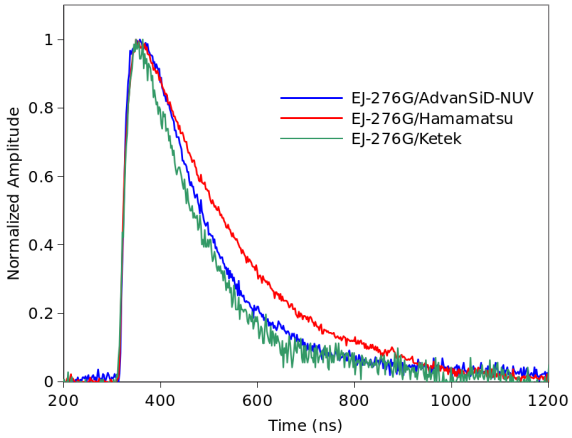

Fig. 6. Typical waveforms of the EJ-276G scintillator coupled to the Hamamatsu, AdvanSiD-NUV, and Ketek SiPM arrays. The signals correspond to an event of 477.4 keV, so the Compton edge of a 661.7 keV γ-ray.

B. Energy and Time Performance

The overvoltage applied to each configuration of scintillator/SiPM arrays was fine-tuned based on the energy resolution optimization. The most favorable performance was achieved at the voltages listed in Table III. The initial voltage used corresponded to the breakdown voltage specified in the product datasheet of each SiPM array. Subsequently, the overvoltage was adjusted within the specified range provided in the product datasheet.

The energy resolution was determined using the Compton coincidence technique, as detailed in Subsection II-E. An illustration of the results for one of the configurations can be observed in Fig. 7. In Fig. 7a, it can be seen the energy spectrum of the $LaBr_3$:Ce detector in coincidence, where a series of red lines represent the energy selection corresponding to the full-energy peak of back-scattered γ-rays at approximately 184.3 keV. Then, in Fig. 7b, the energy spectrum of the EJ-276G/Hamamatsu SiPM array assembly is presented, along with the energy spectrum of events coinciding with the full-energy events of the back-scattered γ-rays, outlined with a green line. To determine the energy resolution at 477.4 keV, the latter spectrum was fitted with a Gaussian function. The energy resolution values achieved for each configuration are presented in Table IV. Notably, the Hamamatsu SiPM exhibits superior performance, especially when it is coupled to the liquid scintillator. In this specific case, the Hamamatsu SiPM demonstrates an energy resolution improvement of approximately 45% higher with respect to the AdvanSiD and Ketek configurations.

TABLE III
BIAS VOLTAGE APPLIED TO EACH SCINTILLATOR/SIPM ARRAY CONFIGURATION

Scintillator/SiPM array	OV (V)	Bias Voltage (V)
EJ-276G/AdvanSiD	4	30
EJ-276G/Hamamatsu	2.75	40.75
EJ-276G/Ketek	4.25	29
EJ-309/AdvanSiD	3.5	29.5
EJ-309/Hamamatsu	2.75	40.75
EJ-309/Ketek	3.75	28.5

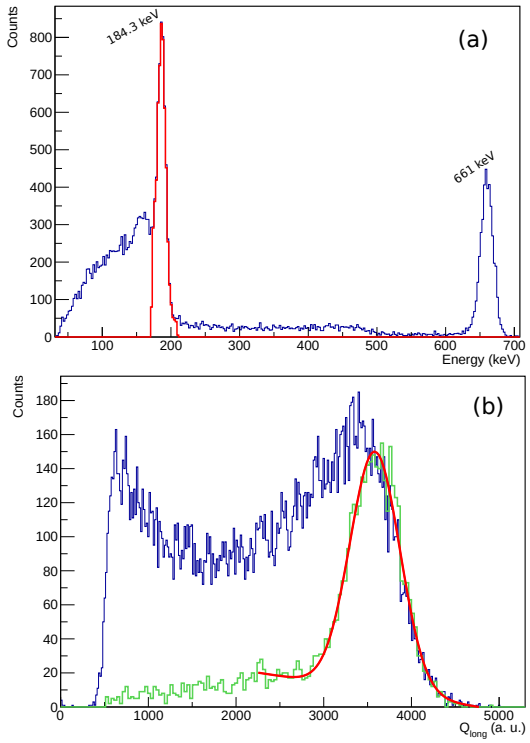

Fig. 7. Energy spectra corresponding to the ^{137}Cs coincidence experiment between the $LaBr_3$:Ce detector (a) and the EJ-276G/Hamamatsu SiPM array asssembly (b).

For the time resolution determination using the ^{22}Na source, we conducted an offline analysis of the waveforms. The parameters of the Digital Constant Fraction Discrimination (DCFD) were optimized to achieve the best time resolution. The best configuration was determined to be a 50% fraction for the scintillator/SiPM array assemblies, featuring a 120 ns of delay for both Hamamatsu and AdvanSiD, an 80 ns of delay for Ketek, and a 25% fraction for the $LaBr_3$:Ce detector along with a 20 ns of delay. Subsequently, we applied a filter by selecting the energy ranges of interest in each detector's spectrum, corresponding to the 511 keV peak for the $LaBr_3$:Ce detector and all events with energies greater than 200 keV for the organic detector. A Gaussian fit was performed on the time spectrum to obtain the total time resolution (FWHM) of the system. The total time resolution is calculated using the formula: $FWHM^2_{total} = FWHM^2_{LaBr_3} + FWHM^2_{Scintillator/SiPM}$. The time resolution of the $LaBr_3$:Ce detector was previously measured as (0.366 $\pm$ 0.002) ns, allowing us to determine the time resolution of the scintillator/SiPM array for each assembly using the same procedure.

This article has been accepted for publication in IEEE Transactions on Nuclear Science. This is the author's version which has not been fully edited and content may change prior to final publication. Citation information: DOI 10.1109/TNS.2024.3387075

Fig. 8 and Fig. 9 shows the time spectra corresponding to each configuration of the scintillator/SiPM array when employing an ^{22}Na source. Subsequently, Table IV presents the time resolution values for each scintillator/SiPM array configuration. Once again, it is evident that the Hamamatsu SiPM outperforms the other SiPM arrays, particularly when paired with the liquid scintillator, the time resolution of the EJ-309/Hamamatsu configuration exhibits a remarkable improvement, decreasing by 56% and 59% when compared to the AdvanSiD and Ketek configurations, respectively.

TABLE IV
VALUES OF THE ENERGY AND TIME RESOLUTION OBTAINED FOR EACH SCINTILLATOR/SIPM ARRAY CONFIGURATION

Scintillator/SiPM array	Energy Resolution (%)	Time resolution (ns)
EJ-276G/AdvanSiD-NUV	29.0±0.2	1.80 ± 0.01
EJ-276G/Hamamatsu	18.8±0.4	1.043 ± 0.003
EJ-276G/Ketek	25.5±0.2	2.33 ± 0.02
EJ-309/AdvanSiD-NUV	20±2	1.17 ± 0.01
EJ-309/Hamamatsu	10.8±0.4	0.517± 0.004
EJ-309/Ketek	19.7±0.2	1.26± 0.01

C. Neutron/γ-ray discrimination capability

We explored the discrimination capability of each combination of scintillator and SiPM array by employing an ^{241}Am-^{9}Be source and the double integration method, as detailed in Subsection II-F. Initially, we conducted the optimization of the short and long integration gates for each assembly, seeking to identify the maximum value of the Figure of Merit (FoM). Subsequently, for each configuration, we generated 2D-PSP and PSP plots. The 2D-PSP plot represents a two-dimensional histogram of PSP values plotted against Q_{long} values. The PSP distribution plot comprised events falling within a light output range corresponding to the Compton edge associated with the 661.7 keV γ-ray emission from ^{137}Cs. The FoM value was computed by analyzing the PSP distribution, as explained in Subsection II-F.

Fig. 10 illustrates the 2D-PSP and PSP plots for the EJ-276G coupled with the Hamamatsu SiPM array, using an ^{241}Am-^{9}Be source. In the 2D-PSP plot, the events used for constructing the PSP distribution are highlighted in a red box. Fig. 11 and Fig. 12 display the 2D-PSP plots associated with each configuration of the scintillator and SiPM array. Table V provides the FoM values and the optimized values for w_{long} and w_{short} for each configuration. Notably, the FoM value for the Hamamatsu configuration when it is coupled to the EJ-309 outperforms the AdvanSiD-NUV and the Ketek results, exhibiting an improvement of 43% and 50% respectively.

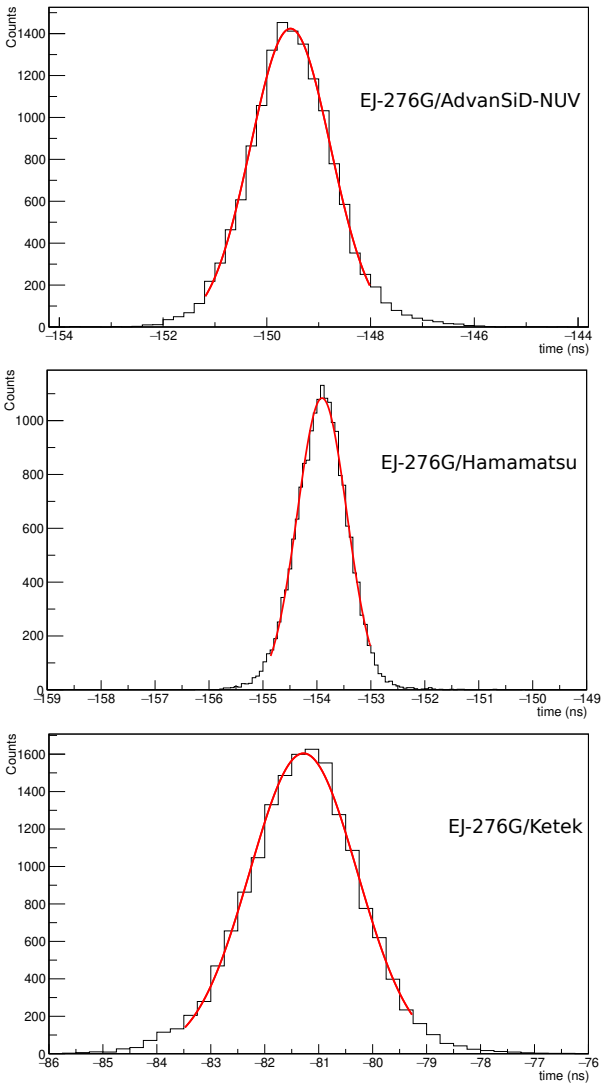

Fig. 8. Time spectra corresponding to the plastic scintillator (EJ-276G) coupled to each SiPM array, using an ^{22}Na source.

TABLE V
OPTIMIZED INTEGRATION WINDOWS (w_{long} AND w_{short}), AND FOM VALUES OBTAINED FOR EACH SCINTILLATOR/SIPM ARRAY CONFIGURATION

Scintillator/SiPM array	w_{long} (ns)	w_{short} (ns)	FoM
EJ-276G/AdvanSiD-NUV	904	240	0.76 ± 0.02
EJ-276G/Hamamatsu	590	220	1.19 ± 0.02
EJ-276G/Ketek	810	176	0.597 ±0.004
EJ-309/AdvanSiD-NUV	586	122	1.15 ± 0.01
EJ-309/Hamamatsu	730	180	2.04 ± 0.01
EJ-309/Ketek	738	190	1.010 ±0.003

D. Discussion of the results

The Hamamatsu SiPM array exhibited superior performance across all studied parameters in all the configurations. This outcome can be attributed to the array's larger surface area, allowing for the collection of more light per event and, as a consequence, creating more photoelectrons per event. Specifically, the Hamamatsu array covers the entire surface of the plastic scintillator and approximately 28% of the liquid scintillator window's surface area. In contrast, the AdvanSiD and Ketek arrays cover about 51% and 28% of the plastic scintillator's surface area, and approximately 13% and 7% of the liquid scintillator's window surface area, respectively. However, it's essential to note that while the surface area is a significant factor in the performance of a SiPM array, other intrinsic characteristics of the SiPM can also influence their performances (photon detection efficiency, dark counts, cross-

This article has been accepted for publication in IEEE Transactions on Nuclear Science. This is the author's version which has not been fully edited and content may change prior to final publication. Citation information: DOI 10.1109/TNS.2024.3387075

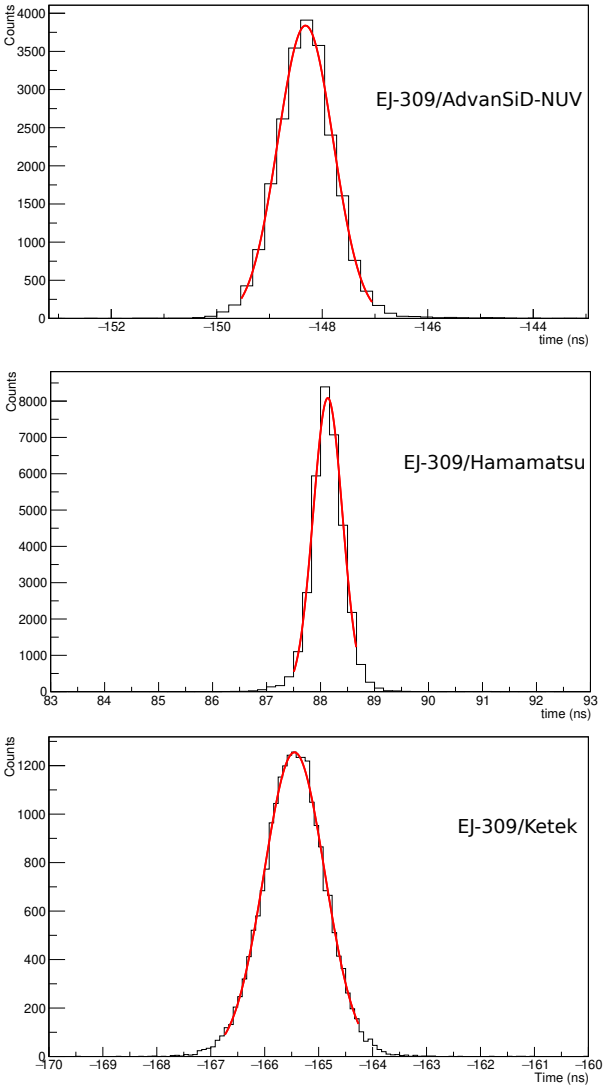

Fig. 9. Time spectra corresponding to the liquid scintillator (EJ-309) coupled to each SiPM array, using an ^{22}Na source.

talking, after pulses, etc.).

In order to compare in an absolute way the reported results in the previous sections, an analysis taking into account the number of photoelectrons created in each scintillator/SiPM configuration is presented. The number of photoelectrons generated for each scintillator/SiPM arrray configuration, N_{phe}, can be estimated using the following equation [25]:

$$N_{phe} = L.O. \times E \times PDE_{int} \times \varepsilon_{L.C.} \quad (1)$$

where $L.O.$ is the light output per unit of energy deposited by electrons of the respective scintillator. According to the producer, for the EJ-309, this value is 12300 photons per 1 MeV electron, while for the EJ-276G it is 8000 photons per 1 MeV electron. E is the energy of the electrons creating light inside the scintillator (E = 0.477 MeV is the one corresponding to the Compton edge of the 0.662 MeV gamma-ray emitted by the ^{137}Cs source). The term PDE_{int} is the integrated Photon Detection Efficiency of each SiPM corresponding to

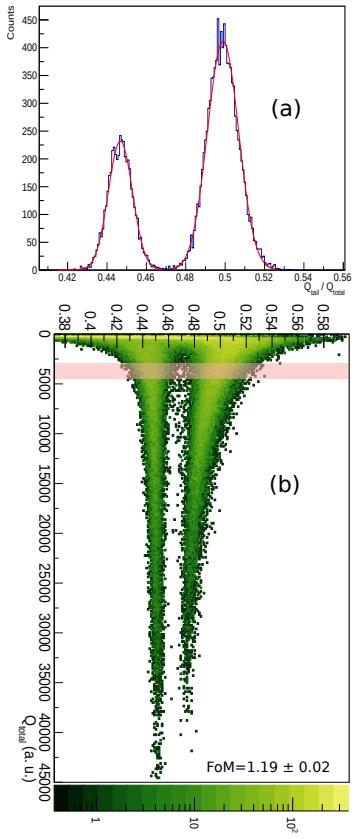

Fig. 10. 2D-PSP (a) and PSP (b) plots corresponding to the EJ-276G coupled to the Hamamatsu SiPM array, using an ^{241}Am-^{9}Be source.

the overvoltage used. And finally, there is the efficiency related to the light collection of each scintillator/SiPM array assembly ($\varepsilon_{L.C.}$). This encompasses the fraction of light reflected in the walls of the scintillator that reaches the scintillator window, the fraction of the window area covered by the SiPM array, the self-attenuation of light by the scintillation material, etc. Being all these processes very complex, the light collection efficiency for each configuration was determined through a semi empirical method. First, a gain calibration of the Advansid and the Ketek arrays with respect to the Hamamatsu was perform. This was done by considering that the response of each SiPM array is as follows [26]:

$$S_{out} = N_{phe} \cdot M + S_{dark} \quad (2)$$

where S_{out} represents the output signal (pulse-height or integral of the pulse) of a specific event. In our set-up it is equivalent to the Q_{total} value. N_{phe} is the number of photoelectrons, S_{dark} is the detector output charge not generated due to the photoelectric effect, and M is the gain, a particular parameter for each SiPM array. For this calculation, we assumed S_{dark} to be negligible. Experimental observations hold this assumption. By performing measurements using a ^{137}Cs source and a LYSO:Ce scintillator (small cube of 10 mm $\times$ 10 mm $\times$ 10 mm), the ratios $M_{Ketek}/M_{Hamamatsu}$ and $M_{AdvanSiD}/M_{Hamamatsu}$ were obtained.

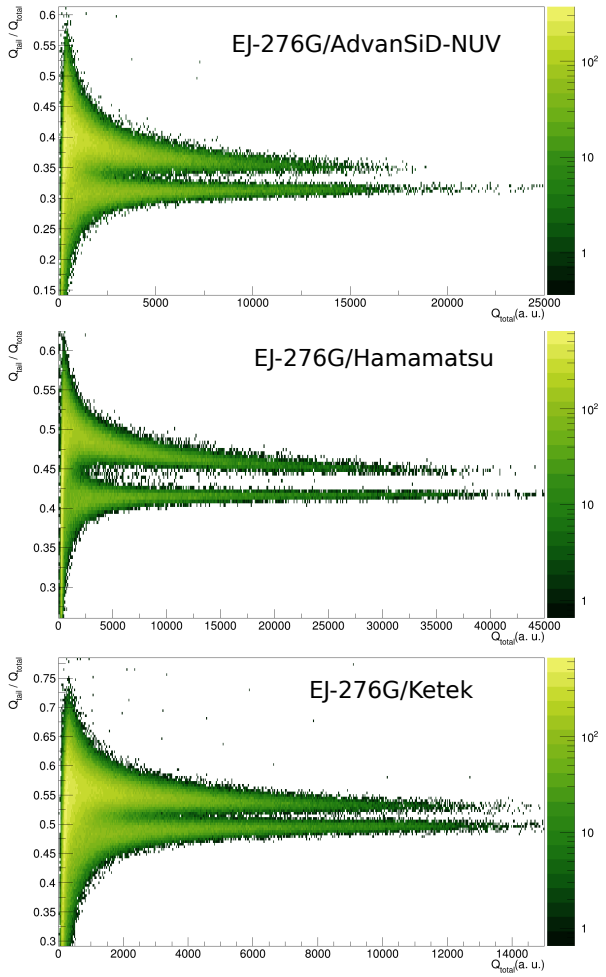

Fig. 11. 2D-PSP plots corresponding to the plastic scintillator (EJ-276G) coupled to three SiPM arrays, using an ^{241}Am-^{9}Be source.

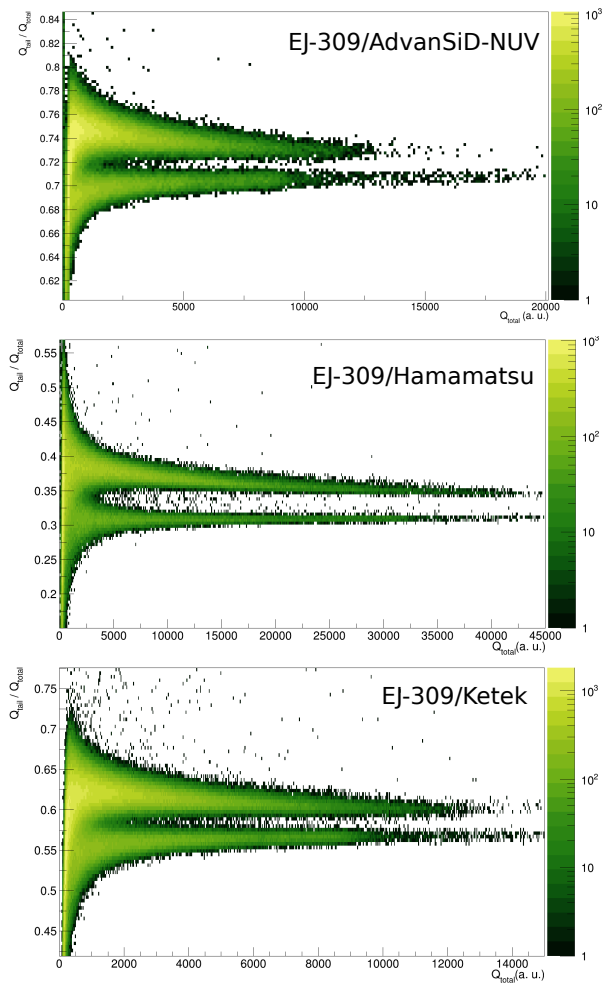

Fig. 12. 2D-PSP plots corresponding to the liquid scintillator (EJ-309) coupled to three SiPM arrays, using an ^{241}Am-^{9}Be source.

Then, operating the SiPM arrays at the same overvoltage used for the gain calibration with the LYSO:Ce scintillator, measurements of the Compton edge position of the 662 keV gamma-ray (^{137}Cs source) with each organic scintillator/SiPM assembly were performed. In this way, by applying eq. 2 and 1 to each measurement, and assuming the $\varepsilon_{L.C.}$ of the EJ-276G/Hamamatsu assembly to be 95% (0.95), the others light collection efficiencies can be determined. This is a very conservative assumption considering that the Hamamatsu SiPM array covers the entire scintillator area, the reflector, consisting of four layers of polytetrafluoroethylene (PTFE) tape, is good enough to reflect most of the light produced in an event, and the light attenuation length of this material is much larger that the dimensions of the scintillator. Larger uncertainties are coming from the data reported by the producers (light output and emission spectra of the scintillators and photon detection efficiency curves). However, in overall, the associated uncertainty is not larger than 10 %.

In the second column of Table VI the number of photoelectrons determined using eq. 1 for each scintillator/SiPM array configuration corresponding to the events of 0.477 MeV (Compton edge of the 0.662 MeV gamma-ray) are given. The energy resolution exhibited by a scintillation detector can be expressed mainly by four terms: the intrinsic resolution of the scintillator (non-proportional response), the transfer resolution (quality of reflective material and optical coupling between scintillator and photodetector), normally this component is negligible with respect to the other terms, the noise contribution, and the statistical contribution of the photoelectrons [27]. In our case, using always the same scintillators, if the obtained energy resolution values are normalized to the number of photoelectrons created, the resulting differences will be mainly ascribed to the noise contribution of the SiPM (the readout board is the same for the three studied SiPM arrays). The limiting resolution solely based on statistical fluctuations in the number of photoelectrons created in the SiPM array yields the following energy resolution: $R_{E|stat} = \frac{2.35}{\sqrt{N_{phe}}}$ [28]. This means that by multiplying the energy resolution values by the square root of the N_{phe}, a constant equal to 2.35 should be obtained, if the rest of the terms that contribute to the energy resolution are negligible (intrinsic resolution of the scintillator, electronic noise, particularly after-pulsing and

cross-talk [10], [27]). In the third column of Table VI the results are reported. As can be seen, the Ketek SiPM array shows the best performance in terms of energy resolution for both scintillators. AdvanSiD performs better than Hamamatsu only when it is coupled to the plastic, while both SiPM arrays perform similarly when coupled to the liquid. The configuration with the EJ-309/Ketek yields the result closest to the value of 2.35. In this case, it can be concluded that the energy resolution is more influenced by statistical fluctuations, suggesting a low contribution of electronic noise compared to the other configurations. The obtained values for the plastic are larger probably due to the non-proportional response of this scintillation material. It is worth mentioning that the EJ-276G is an EJ-276D scintillator with a secondary dye (wavelength shifter) added, which can introduce this kind of behavior. Despite the Ketek array covering the smaller area in both detector configurations compared to the other two arrays, resulting in the generation of fewer photoelectrons, the detectors assembled using the Ketek array perform better, in terms of energy resolution, to the ones assembled with the AdvanSiD array. These results suggest that if a Ketek array would cover the same area as the AdvanSiD (or Hamamatsu) array, it would likely achieve a better energy resolution (with respect to the AdvanSiD or Hamamatsu option).

It is known that the best timing performance is obtained for the fastest detector's signals, in our case, i.e. organic scintillators coupled to a SiPM array, rising times are similar (as shown in Fig. 6), so, the signals generated with the greatest number of photoelectrons will be demonstrated superior timing properties [28]. This fact is verified by looking at the results given in Table IV. However, if one wants to compare the results obtained using the studied SiPM arrays, one can proceed similarly to the energy resolution, so, multiplying the obtained time resolution by the square root of the photoelectrons generated. The outcomes of this multiplication are outlined in the fourth column of Table VI, where the result with the lowest value shows a better performance. It is important to remark that the energy, E, is used to estimate the number of photoelectrons, according to eq. 1, was the average energy of the events considered for the time resolution determination for each detector assembly. The values obtained suggest that the performance of the Hamamatsu array overcomes the one of the other two arrays. However, the AdvanSiD array coupled to the plastic, and the Ketek array coupled to the liquid exhibit similar performances to the Hamamatsu based assemblies. So, it is very likely that arrays with similar active areas will produce similar results. Obviously, the differences between the plastic and liquid results are related to the intrinsic timing properties of the scintillation materials.

Best neutron-γ-ray discrimination capability with organic scintillators is associated with the number of photoelectrons created per pulse, as verified by the results given in Table V. However, normalizing the results by the number of photoelectrons, following the approach used by [21], one can obtain a value that can let the comparison performance between the studied SiPM arrays. So, the FoM value for each scintillator/SiPM array configuration was divided by the square root of the number of photoelectrons ($\sqrt{N_{phe}}$) created. The results are presented in column fifth of Table VI. Notably, the performances are very similar considering the results of a particular scintillator. Meaning that the number of photelectrons is the crucial parameter to take into account to achieved better performance in terms of particle discrimination.

It's noteworthy that the number of photoelectrons calculated using the semi-empirical method yielded a surprisingly higher value than anticipated. This unexpected finding warrants further investigation. For instance, comparing the EJ-276G/Hamamatsu, where the entire detector area is covered, to the liquid scintillator, which covers only 28% of the detector area, one might assume that the loss of light is proportional to the uncovered area. Intuitively, considering the respective light outputs of each scintillator and the fraction of area covered, one would expect the difference in the number of photoelectrons to be approximately 2.3 times higher in favor of the plastic scintillator. However, the semi-empirical calculation reveals a factor of only 1.1, suggesting a non-linear behavior in the collected light, regardless of the coverage area.

TABLE VI
NUMBER OF PHOTOELECTRONS (N_{phe}) CREATED IN EACH SCINTILLATOR/SIPM ARRAY CONFIGURATION ASSOCIATED TO 0.477 MEV EVENTS, ENERGY AND TIME RESOLUTIONS MULTIPLIED BY $\sqrt{N_{phe}}$, AND THE FOM VALUE DIVIDED BY $\sqrt{N_{phe}}$

Assembly	N_{phe}	$R_E \cdot \sqrt{N_{phe}}$	$R_T \cdot \sqrt{N^*_{phe}}$	$\frac{FoM}{\sqrt{N_{phe}}} \times 10^{-2}$
EJ-276G/AdvanSiD	555	6.8 ±0.4	25.6±1.4	3.2±0.2
EJ-276G/Hamamatsu	1611	7.5±0.5	25.3±1.3	3.0±0.2
EJ-276G/Ketek	471	5.5±0.3	30.5±1.8	2.8±0.2
EJ-309/AdvanSiD	504	4.5±0.7	16.2±0.9	5.1±0.3
EJ-309/Hamamatsu	1440	4.1±0.4	12.1±0.7	5.4±0.3
EJ-309/Ketek	317	3.5±0.2	13.8±0.8	5.7±0.3

* The number of photoelectrons are associated to the average energy of the events considered for the time resolution determination

IV. CONCLUSIONS

In this research, we conducted a comparative analysis of two of the most currently promising organic scintillation materials coupled to three different SiPM arrays, focusing on their performance in terms of energy resolution, time resolution, and their capability to discriminate between fast neutrons and γ-rays. Specifically, the SiPM arrays examined in our investigation include the AdvanSiD hybrid array ASD-NUV4S-P-4x4TD (17 mm x 17 mm), the MPPC Hamamatsu S14161-6050HS-04 (24 mm x 24 mm), and the Ketek PA3325-WB-0404 (13 mm x 13 mm). The two organic scintillators used were a plastic scintillator EJ-276G (25 mm dia. x 25 mm thick) and a liquid scintillator EJ-309 (50 mm dia. x 50 mm thick), both from Eljen Technology, Texas USA. Both possess good n/γ-rays discrimination capabilities.

The objective of this work is to offer a comprehensive performance assessment of these six configurations. By doing so, we aim to contribute to a better understanding of the capabilities and limitations of SiPM arrays. Given the increasing popularity of SiPMs in both research and applications, it is important to have a thorough understanding of their characteristics to make well-informed decisions when selecting and utilizing these devices.

To assess both energy and time resolution, we conducted a coincidence experiment employing a $LaBr_3$:Ce detector. The energy resolution was determined through the application of a Compton coincidence technique. In this technique, the energy resolution of each configuration was measured at 477.4 keV, which represents the energy deposited by a 661.7 keV γ-ray (originating from a ^{137}Cs source) after undergoing a back-scattering interaction within the detector's active volume. While, time resolution was determined using a ^{22}Na source, by measuring in coincidence the 511 keV annihilation gamma-rays. On the other hand, the examination of the discrimination capability involved the utilization of a n/γ-ray source, specifically an ^{241}Am-^{9}Be source.

Among all the configurations investigated, the ones based on the Hamamatsu SiPM array exhibited the most outstanding performance. And of course, this is due to the fact that by covering the largest window surface, largest number of photoelectrons per pulse is generated. In particular, it achieved an energy resolution of approximately 10%, a time resolution of 0.52 ns, and a FoM value of approximately 2, when it was coupled to the EJ-309 liquid scintillator.

However, when comparing the obtained results normalizing by the number of photoelectrons created in each SiPM array, the Ketek SiPM array outperformed in terms of energy resolution and demonstrated comparable performance in terms of time resolution and neutron/gamma-ray discrimination capability compared to the AdvansSiD and Hamamatsu arrays. These results lead to the conclusion that, for example, if the Ketek array had the same active area as the AdvanSiD or Hamamatsu arrays, it would likely outperform the results given by those, especially if it is coupled to scintillators such as CLLB, CLYC, etc. where energy resolution and particle discrimination are their most important features.

Additionally, it's worth noting that in this specific study, the plastic scintillator (EJ-276G) exhibited better discrimination performance between neutrons and gamma-rays when coupled to the studied SiPM arrays compared to when coupled to a commercial PMT, as confirmed in one of our previous works [12].

REFERENCES

[1] E. Roncali and S. R. Cherry, "Application of silicon photomultipliers to positron emission tomography," *Annals of Biomedical Engineering*, vol. 39, no. 4, pp. 1358–1377, Apr. 2011.

[2] D. Guberman, J. Cortina, J. Ward, E. Do Souto Espiñera, A. Hahn, and D. Mazin, "The Light-Trap: A novel concept for a large SiPM-based pixel for Very High Energy gamma-ray astronomy and beyond," *Nuclear Instruments and Methods in Physics Research Section A: Accelerators, Spectrometers, Detectors and Associated Equipment*, vol. 923, pp. 19–25, Apr. 2019.

[3] M. G. Bisogni, A. Del Guerra, and N. Belcari, "Medical applications of silicon photomultipliers," *Nuclear Instruments and Methods in Physics Research Section A: Accelerators, Spectrometers, Detectors and Associated Equipment*, vol. 926, pp. 118–128, May 2019.

[4] M. Grodzicka-Kobylka, M. Moszynski, and T. Szczksniak, "Silicon photomultipliers in gamma spectroscopy with scintillators," *Nuclear Instruments and Methods in Physics Research Section A: Accelerators, Spectrometers, Detectors and Associated Equipment*, vol. 926, pp. 129–147, May 2019.

[5] N. Dinu, "Silicon photomultipliers (SiPM)," in *Photodetectors*. Elsevier, 2016, pp. 255–294.

[6] E. Garutti, "Silicon photomultipliers for high energy physics detectors," *Journal of Instrumentation*, vol. 6, no. 10, pp. C10 003–C10 003, Oct. 2011.

[7] B. Sanaei, M. T. Baei, and S. Z. Sayyed-Alangi, "Characterization of a new silicon photomultiplier in comparison with a conventional photomultiplier tube," *Journal of Modern Physics*, vol. 06, no. 4, pp. 425–433, 2015.

[8] R. M. Preston, J. E. Eberhardt, and J. R. Tickner, "Neutron-gamma pulse shape discrimination using organic scintillators with silicon photomultiplier readout," *IEEE Transactions on Nuclear Science*, vol. 61, no. 4, pp. 2410–2418, Aug. 2014.

[9] "Introduction to SiPM. Technical note," SensL, Tech. Rep., 2017.

[10] M. Grodzicka-Kobylka, T. Szczesniak, and M. Moszyński, "Comparison of SensL and Hamamatsu 4×4 channel SiPM arrays in gamma spectrometry with scintillators," *Nuclear Instruments and Methods in Physics Research Section A: Accelerators, Spectrometers, Detectors and Associated Equipment*, vol. 856, pp. 53–64, Jun. 2017.

[11] A. C. Chergui, E. V. Popova, A. A. Stifutkin, O. Dendene, A. L. Ilyin, S. L. Vinogradov, and O. V. Bychkova, "Experimental comparison of the measurement results of two different silicon photomultipliers and organic scintillator to detect fast neutrons," *Journal of Physics: Conference Series*, vol. 1689, no. 1, p. 012039, Nov. 2020.

[12] F. Pino, J. Delgado, G. Mantovani, L. Pancheri, M. Bello, D. Fabris, C. L. Fontana, M. Polo, V. Ruíz, D. Brunelli, A. Quaranta, and S. Moretto, "Novel detector assembly for Neutron/Gamma-Ray discrimination applications based on large-sized scintillators coupled to large area SiPM arrays," *IEEE Transactions on Nuclear Science*, vol. 69, no. 4, pp. 668–676, Apr. 2022.

[13] A. Gonzalez-Montoro and A. J. Gonzalez, "Performance comparison of large-area SiPM arrays suitable for gamma ray detectors," *Biomedical Physics & Engineering Express*, vol. 5, no. 4, p. 045013, May 2019.

[14] F. Pino, C. Fontana, J. Delgado, D. Fabris, G. Nebbia, M. Turcato, D. Brunelli, L. Pancheri, A. Quaranta, and S. Moretto, "Characterization of a medium-sized CLLB scintillator: Single neutron/gamma detector for radiation monitoring," *Journal of Instrumentation*, vol. 16, no. 11, p. P11034, Nov. 2021.

[15] D. Cester, G. Nebbia, L. Stevanato, F. Pino, L. Sajo-Bohus, and G. Viesti, "A compact neutron–gamma spectrometer," *Nuclear Instruments and Methods in Physics Research Section A: Accelerators, Spectrometers, Detectors and Associated Equipment*, vol. 719, pp. 81–84, Aug. 2013.

[16] M. Taggart and P. Sellin, "Comparison of the pulse shape discrimination performance of plastic scintillators coupled to a SiPM," *Nuclear Instruments and Methods in Physics Research Section A: Accelerators, Spectrometers, Detectors and Associated Equipment*, vol. 908, pp. 148–154, 2018.

[17] M. L. Ruch, M. Flaska, and S. A. Pozzi, "Pulse shape discrimination performance of stilbene coupled to low-noise silicon photomultipliers," *Nuclear Instruments and Methods in Physics Research Section A: Accelerators, Spectrometers, Detectors and Associated Equipment*, vol. 793, pp. 1–5, 2015.

[18] F. Shen, Y. Pan, Q. Fu, S. Lin, T. Huang, and W. Wang, "PSD performance of EJ-276 and EJ-301 scintillator readout with SiPM array," *Nuclear Instruments and Methods in Physics Research Section A: Accelerators, Spectrometers, Detectors and Associated Equipment*, vol. 1039, p. 167148, Sep. 2022.

[19] J. Boo, M. D. Hammig, and M. Jeong, "Pulse shape discrimination using a stilbene scintillator array coupled to a large-area SiPM array for hand-held dual particle imager applications," *Nuclear Engineering and Technology*, vol. 55, no. 2, pp. 648–654, 2023.

[20] M. L. Ruch, M. Flaska, and S. A. Pozzi, "Pulse shape discrimination performance of stilbene coupled to low-noise silicon photomultipliers," *Nuclear Instruments and Methods in Physics Research Section A: Accelerators, Spectrometers, Detectors and Associated Equipment*, vol. 793, pp. 1–5, 2015.

[21] M. Grodzicka-Kobylka, T. Szczesniak, M. Moszyński, L. Swiderski, D. Wolski, J. Baszak, S. Korolczuk, and P. Schotanus, "Study of n - γ discrimination by zero-crossing method with SiPM based scintillation detectors," *Nuclear Instruments and Methods in Physics Research Section A: Accelerators, Spectrometers, Detectors and Associated Equipment*, vol. 883, pp. 159–165, Mar. 2018.

[22] C. L. Fontana, M. Lunardon, F. E. Pino, L. Stevanato, A. Carnera, C. Sada, F. Soramel, and S. Moretto, "A distributed data acquisition system for signal digitizers with on-line analysis capabilities," in *2017 IEEE Nuclear Science Symposium and Medical Imaging Conference (NSS/MIC)*. Atlanta, GA: IEEE, Oct. 2017, pp. 1–5.

[23] C. L. Fontana, A. Carnera, M. Lunardon, F. E. Pino, C. Sada, F. Soramel, L. Stevanato, and S. Moretto, "A distributed data acquisition system for

nuclear detectors," *International Journal of Modern Physics: Conference Series*, vol. 48, p. 1860118, Jan. 2018.

[24] L. Swiderski, M. Moszynski, W. Czarnacki, J. Iwanowska, A. Syntfeld-Kazuch, T. Szczesniak, G. Pausch, C. Plettner, and K. Roemer, "Measurement of Compton edge position in low-Z scintillators," *Radiation Measurements*, vol. 45, no. 3, pp. 605–607, Mar. 2010.

[25] A. Ghassemi, K. Sato, and K. Kobayash, "A technical guide to silicon photomultipliers (MPPC) - overview | hamamatsu photonics," Mar. 2017.

[26] "A technical guide to silicon photomultipliers (MPPC) - section 2 Hamamatsu, Photonics." [Online]. Available: https://hub.hamamatsu.com/us/en/technical-notes/mppc-sipms/a-technical-guide-to-silicon-photomutlipliers-MPPC-Section-2.html

[27] M. Grodzicka-Kobylka, T. Szczesniak, M. Moszyński, S. Korolczuk, J. Baszak, and M. Kapusta, "Characterization of large TSV MPPC arrays (4 × 4 ch and 8 × 8 ch) in scintillation spectrometry," *Nuclear Instruments and Methods in Physics Research Section A: Accelerators, Spectrometers, Detectors and Associated Equipment*, vol. 869, pp. 153–162, 2017.

[28] G. F. Knoll, *Radiation detection and measurement*. New York: Wiley, 1979.